Characterization of CCDs with enhanced UV response

Bonanno, Giovanni, Cali, Antonio, Di Benedetto, Rosario, Scuderi, Salvatore

Giovanni Bonanno, Antonio Cali, Rosario Di Benedetto, Salvatore Scuderi, "Characterization of CCDs with enhanced UV response," Proc. SPIE 1743, EUV, X-Ray, and Gamma-Ray Instrumentation for Astronomy III, (8 October 1992); doi: 10.1117/12.130684

SPIE.

Event: San Diego '92, 1992, San Diego, CA, United States

Characterization of CCDs with enhanced UV response

Giovanni Bonanno, Antonio Calì, Rosario Di Benedetto
Catania Astrophysical Observatory
Viale A. Doria 6, I - 95125 Catania

Salvatore Scuderi
Institute of Astronomy
University of Catania (Italy)
Viale A. Doria 6, I - 95125 Catania

ABSTRACT

In this paper we describe the electro-optical characterization of three types of CCDs manufactured by the English Electric Valve (EEV). The sensitive area of these CCDs is treated in order to enhance the UV response; in particular one is "coronene"-coated, thinned, back-illuminated, one is "lumigen" -coated, front-illuminated, and one is "ion-implanted" thinned, back-illuminated. A technical description of the CCDs and the adopted coating process is given. The CCD characteristics such as the read-out noise, the pixel non-uniformity, the dark current and the quantum efficiency in the 2000 – 10500 Å range, are compared. A cosmic-rays analysis for these CCDs is also given.

1. INTRODUCTION

Remarkable advances have been recently made in producing CCDs. Chips having a read-out noise of less than 5 electrons r.m.s. and excellent Charge Transfer Efficency (CTE) performance are now available. Scientific laboratories[1,2,3,4] (i.e. Jet Propulsion Laboratory - U.S.A.) and manufacturers[5] (i.e. English Electric Valve - England) have made noteworthy efforts to enhance the Ultraviolet response, by using a phosphor film (coronene or lumigen) to coat the CCD surface. Moreover, the technique of ion-implanting and laser annealing has been developed in order to avoid the instabilty of these coatings under vacuum conditions. The backside charging technique is well-known[6]. It allows the use of CCD, in the blue and in the visible, with high efficiency; however, these devices, uncoated, have a very low quantum efficiency at wavelengths shorter than 3900 Å, which may be enhanced by treating the CCD surface.

The aim of this work is to investigate the response in the Ultraviolet region and the electro-optical performances of CCDs manufactured using different techniques, in order to get complete information, on the possible use of a large-area CCD as an imaging sensor in that region.

The main parameters which ultimately determine CCD performances are: the readout noise (ron), the charge transfer efficiency (CTE), the linearity, the short and long term non-uniformity, and the quantum efficiency (QE).

We have tested and compared four CCDs: two back-illuminated coronene coated (CCDBICC1, CCDBICC2), a back-illuminated ion-implanted (CCDBIII), and a front-illuminated lumigen-coated (CCDFILC). The electro-optical performances including the quantum efficiency in the 2000 – 10500 Å range at the selected operating conditions of all CCDs are here presented.

0-8194-0916-2/92/$4.00

2. CCD CHIPS AND SURFACE TREATMENT

We briefly describe the four tested CCDs and the adopted techniques to treat the sensitive area to enhance the UV response. The CCDs can be divided in three types: a) front-illuminated with phosphor coating, b) thinned back-illuminated with phosphor coating and c) thinned back-illuminated ion-implanted.

a) The front-illuminated CCD (coded as CCD02-06-210) has a 385 × 576 pixel format, each pixel being 22 μm square. This CCD is coated by sublimating "lumigen" on the surface in a vacuum chamber. The sublimation techinique is the same used by Bredthauer et al.[7]. We have named this CCD as CCDFILC.

b) The two back-illuminated CCDs are a thinned version of the CCD02-06 series. They have a 350 × 512 pixel area, each pixel being 22 μm square. These are coated by depositing a phosphor film of coronene on the surface. The coating technique is somewhat old and similar to that used at the European Southern Obeservatory (ESO). It consists in dyeing the coronene on the CCD surface and placing the CCD in a vibrating holder to obtain a homogeneus coating.[7]. We have named the CCD we operated many times as CCDBICC1 and the CCD that we operate few times as CCDBICC2.

c) The back-illuminated ion-implanted CCD that is a version of the CCD02-06 sensor, has a 350 × 512 pixel area, each pixel being 22 μm square. In this case the improvement of the quantum efficiency is obtained by implanting boron at a $10^{14} - 10^{15}\ cm^{-2}$ concentration, followed by pulsed laser annealing[5]. This process creates an accumulation layer near the back surface thus generating an electric field that leads the photo-electrons away from the back. This technique is relatively new (improvements are in progress see P. Bailey et al[5]) but the important advantage obtained is the QE stability under vacuum conditions. We have named this CCD as CCDBIII.

3. EXPERIMENTAL APPARATUS

The experimental equipment used to characterize the CCDs consists of a monochromator with a 10 Å resolution which allowed us to cover the 2000 – 8000 Å region, a set of interferential filters (with bandwidths ranging from 50 Å to 100 Å), to reduce monochromator straylight problems and to extend the wavelength region up to 10500 Å, a set of suitable lamps specifically a tungsten lamp (used for $\lambda > 4000$ Å), a mercury and a cadmium spectral lamp (for 2000 Å $< \lambda <$ 4000 Å). We also used integrating spheres to have uniform beams of radiation. Finally for the quantum efficiency measurements we used two NIST calibrated photodiodes as reference detectors : one with UV enhanced response for the 2000 – 4000 Å region and the other one which covers the 3500 – 11000 Å wavelength range. All the components of the apparatus were assembled on an optical bench.

Each CCD was installed inside a liquid Nitrogen dewar with a quartz window and cooled by means of a cold finger; a thermoheater maintaned a stable (within 0.1 K) temperature of 143 K.

The CCD controller is based on a design made at the Catania Astrophysical Observatory[9] and can drive different CCDs at different operating contitions. It enables various CCDs' operating modes and controls the CCD operating temperature and a shutter placed in front of the quartz window. The main features of the controller are summarized in table 1.

CCD CONTROLLER FEATURES	
Maximum readable area	: 4096 × 4096 pixels
A/D Converter	: 12 bit (differen. nonlinearity 13 bit)
CCD temperature	: from -90 to -150 $°C$(0.1$°C$ stability)
Pixel scan time	: from 200 to 80 μs (step 10 μs)
Bias voltages	: adjustable in the range of ± 15 Volts
Phase voltages	: adjustable, also the fall and rise time

Table 1: Main features of the CCD controller.

SIGNAL DESCRIPTION	CCDBICC1,2 Volts	CCDFILC Volts	CCDBIII Volts
Output FET gate (Vog)	2.0	2.0	2.0
Substrate (Vss)	6.1	6.1	6.1
Output FET drain (Vdd)	26.0	29.0	29.0
Reset FET drain (Vrd)	17.0	17.0	17.4
Reset phase (ΦR)	9.9	9.9	9.9
Vertical phases (ΦV)	10.0	10.0	10.0
Horizontal phases (ΦH)	5.0	5.0	5.0

Table 2: CCDs operating conditions.

4. CONVERSION FACTOR AND READOUT NOISE

Some CCD electro-optical parameters depend not only on the CCD manufacturing but also on the electronics driving. For example, the total system gain, that we call "conversion factor", expressed as number of electrons per Analog-to-Digital unit (e/ADU), depends on the CCD output circuit gain, and can be settled adjusting the bias level of the CCD output FET. To drive the CCDs we used the operating conditions reported in table 2.

The load current of the output FET (Iod) is 1 mA and the CCD temperature is settled at 143 K for all CCDs.

The conversion factor was determined following the method described by Gudehus and Hegyi[10]. The basic equation is :

$$\sigma_T^2 = \sigma_R^2 + \sigma_{SH}^2 + \sigma_{SP}^2 \quad (1)$$

where σ_T is the observed total noise, σ_R the readout noise, σ_{SH} the shot noise and σ_{SP} is the spatial noise.

The spatial noise can be removed by averaging many exposures (two are sufficient). It can be shown in fact that the best estimate of the total noise minus the spatial noise is :

$$\sigma_T^2 - \sigma_{SP}^2 = \frac{\sum_i (ADU_1 - ADU_2)_i^2}{2n} \quad (2)$$

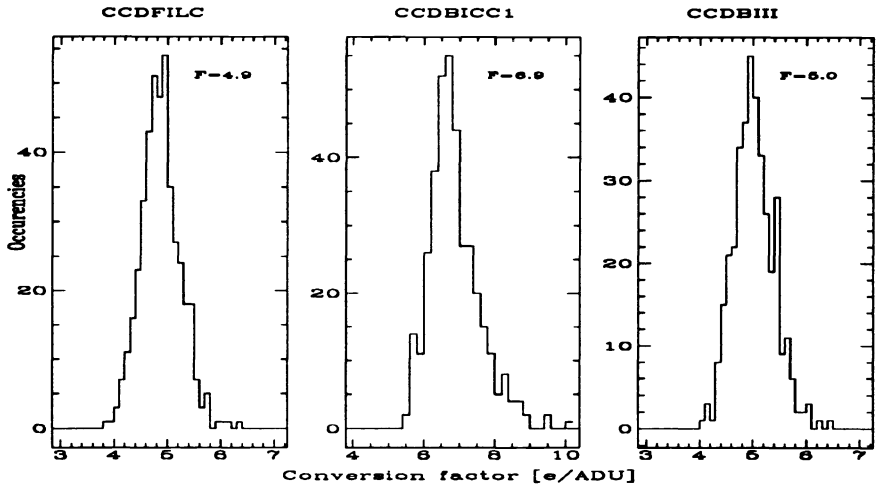

Figure 1: Conversion factor for the three types of CCD.

where ADU_1 and ADU_2 are the numbers of Anolog-to-Digital unit measured on the image 1 and on the image 2 and the sum is over all pixels n in the CCD area considered. Defining the observed signal in ADU as S and the conversion factor as F we can express the shot noise as $\sqrt{S/F}$. The equation (1) became:

$$\sigma_T^2 - \sigma_{SP}^2 = \sigma_R^2 + S/F \tag{3}$$

where the first member is given by equation (2).

Illuminating the CCDs with a stable and uniform radiation source and taking several pairs of images at different exposure times, we determined the difference in equation (2) as a function of the observed signal S and then the conversion factor by means of a linear best fit of the data. The accuracy of this method, which depends on the chosen CCD area which has to be free from artifacts, bad pixels, cosmic rays etc., can be improved dividing the CCD area in 20 × 20 pixel subareas (Janesick[11]) and using for each of these areas the procedure described above to determine the conversion factor. In such a way we obtained the results plotted in histogram form in figure 1.

Even if the method described above allowed us to determine also the readout noise, we decided to compute it from the overscan area, present in all the CCD images, for a better accuracy.

The readout noise was calculated dividing the overscan area in 10 × 10 pixel subareas and computing for each area the standard deviation of the signal. The average of these values multiplied by the conversion factor gives the readout noise. Table 3 summarizes conversion factors and readout noise for all the CCDs.

5. LINEARITY

In order to dermine the CCDs linearity, we used the same series of images as those employed for computing the conversion factor and the read-out noise. We have averaged the pairs of images

CCD Type	Conversion factor F e/ADU	readout noise e $r.m.s.$
CCDBICC1,2	6.9 ± 0.8	9.0
CCDFILC	4.9 ± 0.4	9.7
CCDBIII	5.0 ± 0.4	7.6

Table 3: Conversion Factor and readout noise for all CCDs.

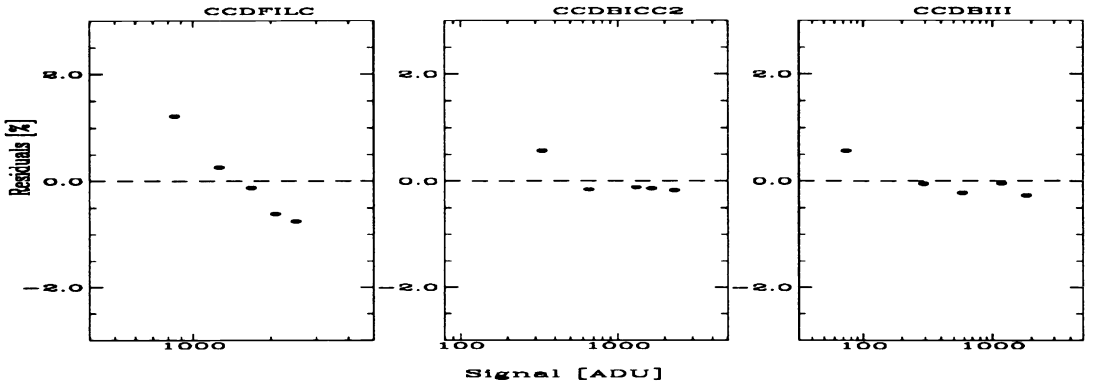

Figure 2: Linearity residuals for all CCDs.

and from the mean image we have chosen a 200 x 200 pixel area, for which we calculated the mean signal. To estimate the deviation from linearity we calculated the linearity residuals as follows:

$$Residuals(\%) = \left(\frac{S/t_{exp}}{\overline{S}} - 1\right) \times 100 \tag{4}$$

where S is the mean signal at the exposure time t_{exp}, and $\overline{S}$ is defined as follows:

$$\overline{S} = \frac{1}{n_{exp}} \sum_i \frac{S_i}{t_{exp_i}}$$

where the sum is over all the couples of images at the different exposure times.

Figure 2 shows linearity residuals as a function of the signal for the three types of CCDs.

As one can see, the linearity of the two back-illuminated CCDs is within 1 %, while the front-illuminated CCD shows a deviation from linearity of 2 %.

6. UNIFORMITY

To study the uniformity of the CCDs response and its colour dependence we used the system shown in figure 3. For $\lambda < 4000$ Å we used the monochromator illuminated by a Hg lamp and

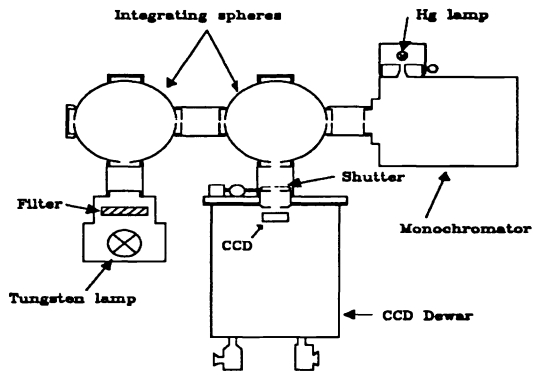

Figure 3: Scheme of the optical system used for the uniformity measurements.

only an integrating sphere, while for $\lambda > 4000$ Å we illuminated the two integrating spheres with a Tungsten lamp and a set of interferential filters.

With this system we illuminated the CCD at λ =2537 Å and in the interval 4000 – 10000 Å (1000 Å step) uniformly.

The pixel-to-pixel variations were calculated dividing the CCDs surfaces in 10 × 10 pixel subareas, resulting in about 1700 subareas. For each area we calculated the mean signal (m) and the standard deviation of the signal (σ) and assumed the pixel-to-pixel nonuniformity to be $2\sigma/m$.

The large-scale variations were obtained measuring the difference between the mean signal in each of 30 × 30 pixel subareas and the mean signal on the entire frame. The uniformity was expressed as the difference between the maximum and the minimum subareas signal divided by the mean level on the entire CCD surface.

The results of this analysis are summarized in figure 4 and in tables 4 and 5. Figure 4 shows the histograms resulting from the pixel-to-pixel variation analysis for three CCDs at $\lambda = 4000$ Å and at $\lambda = 2537$ Å. Each histogram reports the percentage of subareas with respect to their total number as a function of their deviation from uniformity. Table 4, instead, gives the average values of the pixel-to-pixel nonuniformity for the CCDs at the various wavelengths. These values have been obtained through a weighted average of the histograms values. As subareas with bad pixels and cosmic rays have not been rejected, the deviation from uniformity has been overestimated. This is especially true for the images at the shortest wavelengths for which, due to the low quantum efficiency of CCDs and to the intensity of the radiation emitted by the lamps, the exposure times are rather long and the contribution of the cosmic rays gets higher. The contribution of cosmic rays and bad pixels also explains the tails in the histograms. Table 5 summarizes the results of the large-scale uniformity variation. In this analysis, we removed the contribution of bad pixels and cosmic rays.

The data analysis for the CCDFILC shows a small dependence of pixel-to-pixel nonuniformity

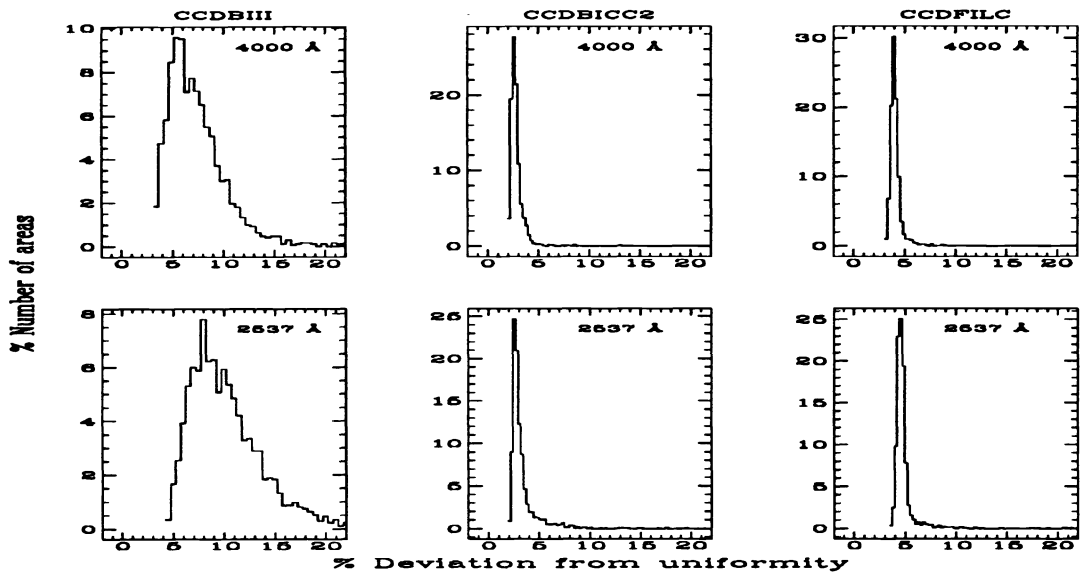

Figure 4: Non-uniformity analysis for all CCDs at 4000 Å and at 2537 Å.

CCD TYPE	2537 Å	4000 Å	5000 Å	6000 Å	7000 Å	8000 Å	9000 Å	10000 Å
CCDBICC1	4.5	4.4	10.5	10.6	10.7	12.3	7.8	6.1
CCDBICC2	2.9	2.7	6.3	7.3	7.5	7.3	6.3	4.3
CCDFILC	4.5	4.0	4.6	3.8	3.3	3.3	3.1	3.4
CCDBIII	9.5	7.2	5.6	3.8	3.4	3.2	3.2	3.2

Table 4: Pixel-to-pixel non-uniformity (%) at different wavelengths for all CCDs.

on wavelength. In fact for $\lambda \leq 5000$ Å the uniformity is a bit lower. At 5000 Å this behaviour is probably due to the polysilicon which can determine a sort of interference in the substrate, resulting in a poorer uniformity. As the coating converts photons of shorter wavelengths to 5000 Å photons, this can explain the lower uniformity at these wavelengths. The large-scale nonuniformity is due to the fact that the central zone of the chip seems to be more sensitive than the peripheral ones. From table 5 we can note that going from shorter to longer wavelength the nonuniformity rises. Furthermore for $\lambda \leq 5000$ Å the uniformity remains constant.

The CCDBICC1 and CCDBICC2 show a similar wavelength dependance of the pixel-to-pixel nonuniformity, but the CCDBICC1 has a poorer uniformity for $\lambda \geq 5000$ Å, due to the strong interferencial fringes, not present at 4000 Å and 2537 Å. The large-scale uniformity has been measured at all wavelengths only for the CCDBICC2. The results shown in table 5 confirm the growing of nonuniformity with wavelengths due to fringes. We measured the large-scale nonuniformity of the CCDBICC1 only at $\lambda = 2537$ and found a rather low uniformity (35 %) compared with the CCDBICC2, which may be attributed to the degradation of the coating.

Finally the CCDBIII, due to the improved thinning technology, shows almost no evidence of fringes. This explain the good small-scale uniformity, comparable to that of CCDFILC for $\lambda \geq$

CCD TYPE	2537 Å	4000 Å	5000 Å	6000 Å	7000 Å	8000 Å	9000 Å	10000 Å
CCDBICC2	20.4	8.2	11.6	14.5	17.6	23.1	28.0	30.3
CCDFILC	6.6	6.7	6.7	8.6	10.5	8.7	10.0	11.3
CCDBIII	68.9	47.4	26.5	8.1	9.7	14.7	16.3	26.3

Table 5: Large-scale non-uniformity (%) at different wavelength for all CCDs.

5000 Å. In contrast, at shorter wavelengths, the uniformity worsens, due to the unsatisfactory laser annealing of the ion-implantation. This behavior is even more evident in the large-scale uniformity.

7. DARK CURRENT AND COSMIC-RAYS

In order to get information on dark current at the operating temperature (143 K), we acquired dark exposures with the integration time increasing from 300 to 2700 seconds. The analysis of the images has produced obscure results; in fact we found evidence of a slight decrease of dark current with respect to the elapsed time from the starting operation. Similar results are obtained for thinned Reticon CCDs by Robinson[13]. For this reason we can give only a superior limit of about 40 $e\ pix^{-1}h^{-1}$ for the CCDFILC and of about 10 $e\ pix^{-1}h^{-1}$ for the three thinned back-illuminated CCDs.

As the cosmic rays are the main limiting factor in determining the longest exposure which can be made with a CCD, it is important that no extra events are introduced by local radioactivity, either in the chip package itself or in the materials of the cryostat. Unfortunately, we have no cosmic rates avaliable to compare with our measurements, so the best we can do is to attribute any excess to an average rate among that obtained for the various CCDs to local (in the sense above specified) radioactivity. To calculate the cosmic rays rate we took three long (at least 20 minutes) dark exposures for each CCD, then we selected an area of 200 × 200 pixels and searched for pixels with a signal higher than the mean signal in the subarea plus five times the standard deviation of the signal. The comparison among the three images allowed us to exclude the contribution of hot pixels. We repeat this procedure for different areas on the CCDs and table 6 gives the average cosmic rays rate, the average charge involved in a single cosmic ray event and the average number of pixels involved in one event for the three CCDs. Figure 5 shows the above mentioned analysis for an integration time of 2400 seconds on the CCDFILC chip.

8. QUANTUM EFFICIENCY IN THE 2000 - 10500 Å RANGE

The method employed to measure the CCD quantum efficiency consists of comparing the signal measured on the CCD with that of a reference photodiode calibrated by the National Institute of Science and Technology (NIST). Figure 6 shows the schematic diagram of the system used to obtain quantum efficiency data.

The photodiode is located in the same place as the CCD and exposed to the same light flux. Since the QE of the diode is known and the signal for each pixel is measured, the QE of the CCD is easily calculated by dividing the CCD signal S_{CCD} in terms of electrons by the photodiode signal S_D in terms of photo-electrons, that is I_D/QE_D. The equation is written as follows:

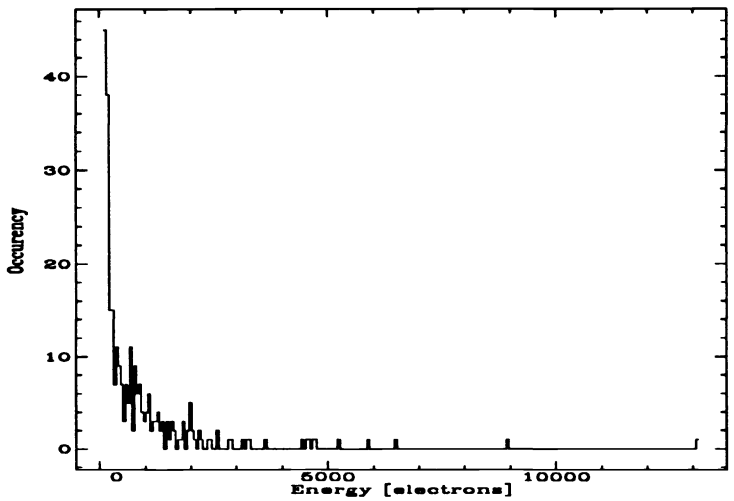

Figure 5: Histogram of cosmic-ray events observed in a 2400-second exposure of dark image.

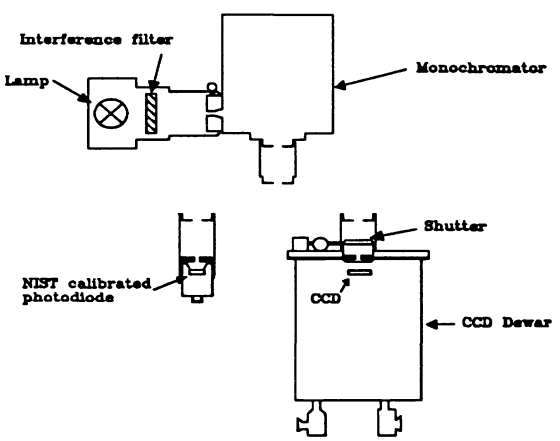

Figure 6: Scheme of the system used for the quantum efficiency measurements.

CCD Type	Cosmic-rays rate *events* $cm^{-2}s^{-1}$	Charge in a single event *electrons*	number of pix involved
CCDBICC1	0.104	1100	3.5
CCDBICC2	0.038	2254	3.5
CCDFILC	0.110	4000	5.0
CCDBIII	0.041	3320	5.0

Table 6: Cosmic rays analysis for all CCDs.

$$QE_{CCD} = \frac{S_{CCD}}{I_D} QE_D$$

where: S_{CCD} is the signal of the CCD pixel (ADU/s $\times F$) in e-/s, I_D is the signal of the photodiode in e-/s, QE_D is the quantum efficiency of the photodiode ($QE_D = 12390 \times \frac{R}{\lambda}$) with R spectral responsivity (Amps/Watt) at the wavelength λ (Å).

As previously said, in order to cover the wavelength range of 2000 – 10500 Å, we illuminated the monochromator with a Cd lamp, a Hg lamp and a Tungsten lamp with a set of interference filters. To be sure that the output light from the monochromator impinging on both detectors is the same, without any loss of signal due to the different geometry of the sensitive area of the detectors, we put a 2-mm pin-hole in front of them.

In calculating the pixel signal, we have taken into account the absorption of the dewar window, constituted by "fused silica" and having a transmittance of about 95 % in the visible and decreasing to about 92 % at shorter wavelengths.

Figure 7 shows the quantum efficiency related to the various CCDs. For the sake of clarity, we decided not to show the errorbars, which are at most not greater than 10 % in the UV region, and much lower at the other wavelengths.

In the 4000 - 10000 Å range all the CCDs, either front- or back-illuminated, show a so-called "typical" QE. In contrast, in the 2000 - 4000 Å range we note a different behaviour for the various CCDs.

The QE of the CCDFILC is higher than 15 % and is almost constant in that spectral range.

The CCDBICC2 shows a QE which is almost twice than the CCDBICC1, demonstrating that the coating is subject to changes with the number of times the CCD is in operation; in fact as written above, the CCDBICC2 has been operated few times.

The QE of the CCDBIII in the range decreases continuosly from 4000 Å and falls to few percents at 2537 Å. This result was unexpected because it contrasts with that reported in literature[14]. We informed the manufacturer about this problem and the EEV replied that this drop-off at that wavelength probably depends on a particular coating that absorbs the radiation down 3000 Å.

9. CONCLUSIONS

This CCD characterization work has pointed that some techniques enhancing the CCD UV response can give encouraging results. The CCDs have shown a deviation from linearity lower than

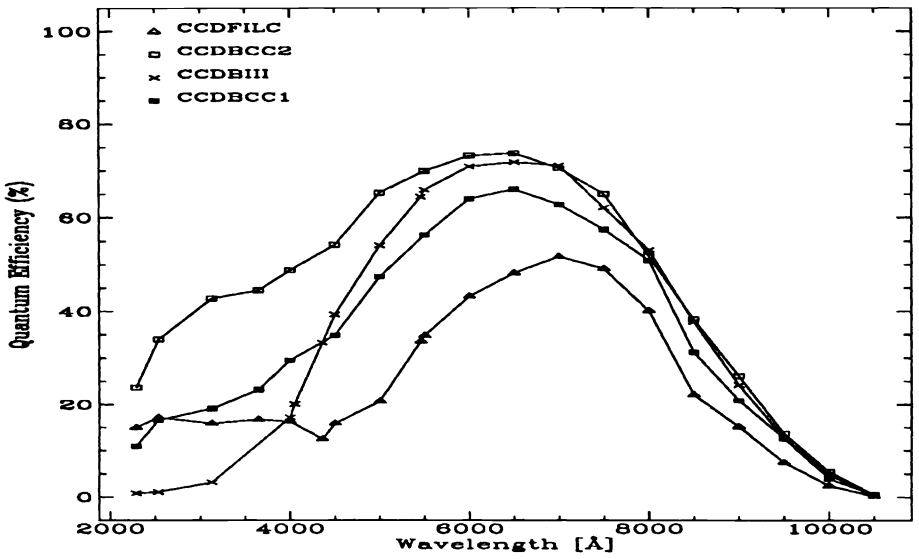

Figure 7: Plots of the quantum efficiency measurements obtained for the four CCDs.

1 % and a readout noise not higher than 9 electrons r.m.s, the CCDFILC has shown a pixel-to-pixel nonuniformity of 3 - 4 % in the considered spectral range, while the CCDBIII has shown a nonuniformity of about 10 % at 2537 Å; the quantum efficiency if, from one side, is acceptable for the CCDFILC in the considered range, on the other side, is unacceptable for the CCDBIII. As regards the two CCDBICC, a remarkable difference of QE has been noted, demonstrating a sort of instability of the coating and its dependency on the number of operations. However, as said before, the UV enhancing techniques are still in progress, also for example in the field of laser-annealing for the ion-implantation. We are confident that in the near future manufacturers can be able to produce detectors with high and very stable QE in the UV region, with a readout noise lower than 3 electrons r.m.s. and with very low percentage of pixel-to-pixel non uniformity in all the spectral range in which CCDs are sensible.

10. ACKNOWLEDGEMNTS

We would like to thank Prof. M. Rodonò director of the Catania Astrophysical Observatory for supporting and encouraging this work. We thank Prof. G. Tondello for providing the monochromator and Mr. G. Gentile and Mr. G. Carbonaro for the realization of some mechanical devices. Finally we thank Miss D. Recupero for the linguistic revision of the paper.

11. REFERENCES

1. J. Janesick, T. Elliot, G. Fraschetti, S. Collins, M. Blouke, B. Corrie, "Charge-Coupled Device pinning technologies", Proc. SPIE 1071, 153-168 (1989).

2. G.R. Sims, F. Griffin, M.P. Lesser, "Improvements in CCD quantum efficiency in the UV and near-IR", Proc. SPIE 1071, 31-42 (1989).

3. M.M. Blouke, M.W. Cowens, J.E. Hall, J.A. Westphal, A.B. Christensen, "Ultraviolet down-converting phosphor for use with silicon CCD imagers", Appl. Opt., Vol. 19, No. 19 (1980).

4. M.W. Cowens, M.M. Blouke, T. Fairchild, J.A. Westphal, "Coronene and liumogen as VUV sensitive coatings for Si CCD imagers: a comparison", Appl. Opt., Vol. 19, No. 22, 3727-3728 (1980).

5. P. Bailey, C. Castelli, M. Cross, P. Van Essen, A. Holland, F. Jansen, P. De Korte, D. Lumb, K. McCarthy, P Pool, P. Verhoeve, "Soft X-ray Performance of Back-illuminated EEV CCDs", Proc. SPIE 1344, 356-371 (1990).

6. J. Janesick, T. Elliot, T. Daud, J. McCarthy, M. Blouke, "Backside charging of the CCD", Proc SPIE 570, 46-80 (1985).

7. R.A. Bredthauer, C.E. Chandler, J.R. Janesick, T.W. McCurnin, G.R. Sims, "Recent CCD Technology Developments", Instrumentation for Ground-Based Optical Astronomy, 486-492 (1987).

8. M. Cullum, S. Deiries, S. D'Odorico, R. Reiss, "Spectroscopy to the Atmospheric Transmission Limit with a Coated GEC CCD", Astron. Astrophys., Vol. 153, L1-L3 (1985).

9. G. Bonanno, R. Di Benedetto, "A CCD Camera for the Echelle Spectrograph at Catania Astrophysical Observatory", P.A.S.P., Vol. 102, 835-841 (1990).

10. D.H. Gudehus, D.J. Hegyi, A.J., Vol. 90,130 (1985).

11. J. Janesick, K. Klaasen, T. Elliot, "Charge-Coupled Device Charge Collection Efficiency and Photon Transfer Technique", Opt. Eng., Vol. 26, No. 10, 972-980 (1987).

12. J. Janesick, T. Elliot, G. Fraschetti, S. Collins, "Charge-Coupled Device Pinning Technologies", Proc. SPIE Vol. 1071, 153-169 (1989).

13. L. Robinson, W. Brown, K. Gilmore, R. Stover, M. Wei, J.C. Geary, "Charge-Coupled Devices and Solid State Optical Sensor II", Proc. SPIE Vol. 1447, 214-228 (1991).

14. R.A. Stern, R.C. Catura, R. Kimble, M. Winzenread, M.M. Blouke, R. Hayes, D.M. Walton, J.L. Culhane, "Ultraviolet and extreme ultraviolet response of charge-coupled-device detectors", Opt. Eng., Vol. 26, No. 9, 875-883 (1987).